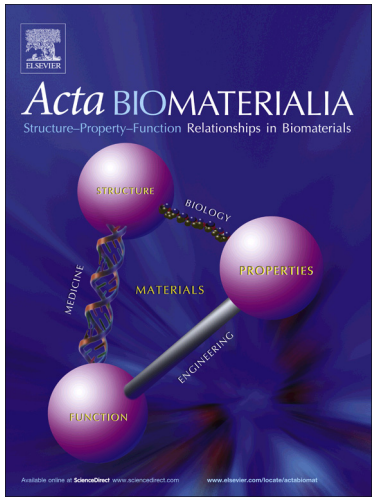

Nanosized sustained-release drug depots fabricated using modified tri-axial electrospinning

Guang-Zhi Yang, Jiao-Jiao Li, Deng-Guang Yu, Mei-Feng He, Jun-He Yang, Gareth R. Williams

PII: S1742-7061(17)30078-8
DOI: http://dx.doi.org/10.1016/j.actbio.2017.01.069
Reference: ACTBIO 4704

To appear in: *Acta Biomaterialia*

Received Date: 9 October 2016
Revised Date: 18 January 2017
Accepted Date: 25 January 2017

Please cite this article as: Yang, G-Z., Li, J-J., Yu, D-G., He, M-F., Yang, J-H., Williams, G.R., Nanosized sustained-release drug depots fabricated using modified tri-axial electrospinning, *Acta Biomaterialia* (2017), doi: http://dx.doi.org/10.1016/j.actbio.2017.01.069

Nanosized sustained-release drug depots fabricated using modified tri-axial electrospinning

Guang-Zhi Yang [a,1], Jiao-Jiao Li [a,1], Deng-Guang Yu [a,*], Mei-Feng He [a], Jun-He Yang [a], Gareth R Williams [b,*]

[a] School of Materials Science & Engineering, University of Shanghai for Science and Technology, 516 Jungong Road, Shanghai 200093, China.

[b] UCL School of Pharmacy, University College London, 29-39 Brunswick Square, London WC1N 1AX, UK.

Corresponding authors:
Prof. Deng-Guang Yu and Dr. Gareth R. Williams

Addresses:
DGY:
School of Materials Science & Engineering,
University of Shanghai for Science and Technology,
516 Jungong Road, Yangpu District,
Shanghai 200093, P.R. China
Tel: +86-21-55270632
Fax: +86-21-55270632
Email: ydg017@usst.edu.cn

GRW:
UCL School of Pharmacy
University College London
29-39 Brunswick Square
London
WC1N 1AX
Tel: +44 207 753 5868
Email: g.williams@ucl.ac.uk

[1] These authors contributed equally.

Abstract:

Nanoscale drug depots, comprising a drug reservoir surrounded by a carrier membrane, are much sought after in contemporary pharmaceutical research. Using cellulose acetate (CA) as a filament-forming polymeric matrix and ferulic acid (FA) as a model drug, nanoscale drug depots in the form of core-shell fibers were designed and fabricated using a modified tri-axial electrospinning process. This employed a solvent mixture as the outer working fluid, as a result of which a robust and continuous preparation process could be achieved. The fiber-based depots had a linear morphology, smooth surfaces, and an average diameter of 0.62 ± 0.07 μm. Electron microscopy data showed them to have clear core-shell structures, with the FA encapsulated inside a CA shell. X-ray diffraction and IR spectroscopy results verified that FA was present in the crystalline physical form. In vitro dissolution tests revealed that the fibers were able to provide close to zero-order release over 36 h, with no initial burst release and minimal tailing-off. The release properties of the depot systems were much improved over monolithic CA/FA fibers, which exhibited a significant burst release and also considerable tailing-off at the end of the release experiment. Here we thus demonstrate the concept of using modified tri-axial electrospinning to design and develop new types of heterogeneous nanoscale biomaterials.

Keywords: Nanoscale drug depot; sustained release; cellulose acetate; tri-axial electrospinning; core-shell nanostructure

1. Introduction

Nanosized drug depots, in which a drug reservoir is surrounded by pharmaceutical excipients, have attracted much attention in the biomedical field recently [1-6]. They have been explored for drug delivery through a variety of administration routes (such as oral, injected, inhaled, and implanted) and also as stents in tissue engineering [7-11]. Two trends are obvious with this type of biomaterials. One is that almost all the depots take the form of nanoparticles, microspheres or microemulsions [12-14]. Another is that the fabrication methods are mainly "bottom-up" approaches, including chemical synthesis, molecular self-assembly and emulsion methods; these are often time-consuming and very difficult to perform on a large scale [15-18]. New approaches for creating this kind of nanostructure, particularly "top-down" methods that can be scaled up easily, would offer great benefit to the fields of biomaterials and pharmaceutics.

One such route is the electrospinning technology, which uses electrical energy to produce nanoscale fiber composites from solutions of a polymer and functional component. After rapid development in the last two decades, the most exciting new work on electrospun fibers falls in two areas. The first is scale-up, with production on an industrial scale now possible. This has mainly been investigated in the context of monolithic fibers with one or two functional ingredients/nanoparticles distributed homogeneously in the filament-forming polymer matrix [19-22]. The second is the creation of more complex nanostructures (such as core-shell and Janus systems, and combinations thereof) in order to yield materials with improved functional

performance [23-26]. In the biomedical field, if a drug reservoir could be formed as the core of electrospun core-shell fibers, then new fiber-based nanoscale drug depots could be created, such as an electrospun suture [27]. These would differ significantly from the nanoparticle-based depots which have mainly been explored to date. In the cases of coaxial and tri-axial electrospinning, it is possible to run these with only one of the working fluids being electrospinnable alone [28, 29]. In standard coaxial electrospinning, the sheath fluid must be electrospinnable to support the electrospinning process and the formation of core-shell structures [30]. However, a modified coaxial electrospinning process, characterized by the utilization of un-spinnable liquids as the sheath working fluids can also be implemented [29,31]. Similarly, traditional tri-axial electrospinning always uses an electrospinnable outer fluid [32-40]. A modified tri-axial process focused on the exploitation of un-spinnable liquids has also been reported [28]. These might comprise solvents, small molecule solutions, emulsions and suspensions, and should lead to a range of novel structures. Thus, it can be hypothesized that these technologies can be exploited to create drug-loaded nanofibers containing drug reservoirs even though the drug itself has no filament-forming properties.

A wide variety of raw materials have been investigated as the shell for encapsulating a core drug reservoir. These materials include the traditional pharmaceutical excipients approved by the FDA such as natural polymers, a range of synthetic polymers, and phospholipids, but also more exotic systems including hydrogels and even inorganic material such as TiO_2 [41-44]. Naturally-occurring

polymers remain a key focus of research interest because of their abundant supply and relatively environmentally-friendly preparation routes. This is reflected in the frequent use of cellulose and its derivatives not only in the scientific literature but also in the food and pharmaceutical industries [45, 46]. In particular, cellulose acetate (CA), the acetate ester of cellulose, has broad applications - for instance in the coatings of pharmaceutical and food products, and as film in photography [47]. CA has been also frequently been utilized as the filament-forming polymer for creating drug-loaded nanofibers through single-fluid electrospinning spinning [48]. However, the direct electrospinning of CA is non-facile because the need to use volatile solvents in this process causes frequent clogging of the spinneret [31]. Furthermore, monolithic drug loaded CA nanofibers tend to exhibit an undesirable initial burst release [49, 50], which inhibits their potential as sustained-release biomaterials.

In this work, with the phytochemical ferulic acid (FA) as a model drug, we explore the preparation of CA-based nanoscale drug depots using a modified tri-axial electrospinning process. As a control, monolithic drug-CA fibers were produced using a modified coaxial process. The fiber morphologies, structures, functional performance, and the distribution and physical form of the drug in the formulations were compared in detail.

2. Experimental section

2.1. Materials

Ferulic acid (FA; purity> 98%) was purchased from the Yunnan Yunyao Lab Co., Ltd. (Kunming, China). CA (M_w=100,000 Da) was obtained from Acros Organics (Geel,

Belgium). Methylene blue, methylene orange, N,N-dimethylacetamide (DMAc), anhydrous ethanol and acetone were obtained from the Shanghai SSS Reagent Co., Ltd. (Shanghai, China). All other chemicals were analytical grade commercial products. Freshly double distilled water was used where required.

2.2. Electrospinning

Three kinds of electrospinning processes (traditional coaxial, modified coaxial and modified tri-axial) were explored for preparing fibers. The outer fluids for modified coaxial and tri-axial electrospinning comprised a solvent mixture of acetone, ethanol and DMAc in a volume ratio of 4:1:1 [30]. For the traditional coaxial process and the modified tri-axial process, an electrospinnable solution of CA (12% w/v in a mixture of acetone, ethanol and DMAc, 4:1:1 v/v/v) was utilized to surround an unspinnable 15% w/v FA solution in acetone/ethanol/DMAc (4:1:1 v/v/v). For the modified coaxial process, the core fluid comprised CA and FA at 12 and 3% w/v in the same solvent system. These experimental conditions are summarized in Table 1.

Each of the working fluids was driven by a syringe pump (KDS100, Cole-Parmer, Vernon Hills, IL, USA). A high voltage generator (ZGF 60kV/2mA, Wuhan Huatian Corp., Hubei, China) was applied to create an electric potential between the spinneret and collector. A flat piece of cardboard wrapped with aluminum foil was used as the collector plate. Both the concentric (coaxial) spinneret and tri-layer spinneret were produced in-house. After a series of initial optimization experiments, the applied voltage and spinneret to collector distance were fixed at 18 kV and 20 cm. The flow rates of the working fluids are listed in Table 1. To aid optimization of the

experimental conditions, 2 μg/mL of methylene blue and methylene orange were added to the inner and middle working fluids, respectively.

Table1

2.3. Characterization

2.3.1. Morphology

The morphology of the fibers and their cross-sections were probed using a Quanta FEG450 field emission scanning electron microscope (SEM; FEI Corporation, Hillsboro, OR, USA). Before examination, samples were sputter-coated with platinum under argon. A polarized optical microscope (XP-700, Chang-Fang Optical Instrument Co., Ltd., Shanghai, China) was used to study the raw drug powders and CA particles. The fiber diameters were estimated from SEM images using the ImageJ software (National Institutes of Health, Bethesda, MD, USA). Samples of fibers for cross-section analysis were prepared immersion in liquid nitrogen for 20 min, after which they were manually broken.

2.3.2. Physical form

X-ray diffraction patterns (XRD) were recorded on a Bruker AXS diffractometer (Bruker, Karlsruhe, Germany). Fourier transform infrared (FTIR) analysis was carried out on a Spectrum 100 FTIR Spectrometer (Perkin Elmer, Billerica, MA, USA). For the latter, samples were prepared using the KBr disc method.

2.3.3. In vitro drug release

FA has a maximum absorbance at λ_{max} = 322 nm [51], and was quantified on a Lambda 950 UV/vis/NIR spectrophotometer (Perkin Elmer, Billerica, MA, USA)

following construction of a calibration curve. The in vitro drug release profiles were measured according to the Chinese Pharmacopoeia (paddle method, 2015 Ed.) using a dissolution apparatus with six cells (RCZ-8A, Tianjin University Radio Factory, Tianjin, China). 40 mg of FA powder (particle size < 20 μm) or 0.2 g of the F2 and F3 fibers (containing the equivalent amount of FA) were placed in 900 mL of phosphate buffered saline (PBS, pH 7.0, 0.1M) at 37 ± 1 ℃, with a 50 rpm rotation speed. All experiments were performed under sink conditions. At pre-determined time points, 5.0 mL of the dissolution liquid was removed for analysis. 5.0 mL of pre-heated PBS was then added to the cells to maintain a constant volume. All experiments were repeated six times, and the results are reported as mean ± S.D.

2.4. Statistical analysis

The experimental data are presented as mean ± SD. The results from the in vitro dissolution tests were analyzed using one-way ANOVA. The threshold significance level was set at 0.05. Thus, p (probability) values lower than 0.05 were considered statistically significant.

3. Results and discussion

3.1. Modified tri-axial electrospinning

Electrospinning is commonly considered to be easy, low-cost and straightforward, giving products that have large surface areas and high porosity. However, the most fascinating aspect of this technique in the authors' view is that complicated nanostructures can easily be created in a "top-down" manner through a single step in double- or multiple-fluid spinning, allowing systems to be accessed which are

difficult or even impossible to achieve from "bottom-up" synthesis processes [52]. The implementation of double- or multiple-fluid processes is similar to the one-fluid process (Fig. 1a), except that more complex spinnerets are required. The introduction of un-spinnable fluids into the process can greatly expand the range of novel functional nanomaterials which can be produced [28]. There are only slightly over 100 polymers which have filament-forming properties in electrospinning, and even these often can only be processed in a very narrow concentration window [53]. Our previous report of modified tri-axial spinning used a pure solvent as the outer fluid, a spinnable Eudragit solution in the center, and an unspinnable drug/phospholipid core, with the aim of generating a colon-targeted delivery system [28]. This comprised a useful proof-of-concept but there are myriad further opportunities to explore, and we expand significantly on this previous work here.

Fig. 1.

Building on our previous investigations [28,29,32], we sought to use tri-axial electrospinning to prepare novel CA-based depot structures in this work (Fig. 1b). In addition to the tri-layer concentric spinneret, a polymer-coated concentric spinneret was applied for carrying out coaxial spinning. Digital images of the concentric and tri-layer spinneret nozzles are shown in Fig. 2a1 to a4. The concentric spinneret is coated with polyvinyl chloride (PVC), an antistatic material. It is able to effectively prevent electrical energy loss to the surroundings. It also helps to prevent interactions between the spinneret and working fluids, and reduces the clogging of the spinneret which can occur as a result of the build-up of solid material on it [54].

The PVC-coated concentric spinneret was found to be rapidly clogged when a traditional coaxial electrospinning experiment was conducted with a 12% w/v CA solution as the shell and a pure FA solution for the core working fluid (Fig. 2b). Thus, the collection of the F1 fibers was abandoned. However, using a co-dissolving solution containing both CA and FA as the core fluid, and a solvent sheath fluid, a modified coaxial process could be implemented to create monolithic FA-loaded CA nanofibers (F2) using the same spinneret (Fig. 2c). The latter processes run smoothly and continuously because of the "lubrication effect" of the sheath solvent mixture. The presence of a surrounding solvent at the exit of spinneret replaces the interfaces between the viscous polymer solution and the atmosphere with a solvent/atmosphere interfaces, which can effectively prevent premature drying and clinging of the working polymer fluid. Thus, with the two-needle spinneret, only monolithic fibers can be generated.

The connections of the tri-layer concentric spinneret to the syringe pumps and the power supply are shown in Fig. 2d. A typical working process under the optimized experimental parameters is depicted in Fig. 2e. A Taylor cone can be seen on the spinneret; this ejects a straight fluid jet, which is followed by numerous gradually enlarged coiled circles. The bottom-right inset of Fig. 2e gives a clear image of the compound Taylor cone with three different fluid layers, as indicated by the color-markers methylene orange and methylene blue. The implementation of a modified tri-axial process could thus lead to the production of core-shell structures, which was not possible through a standard co-axial process owing to the need to have

a lubricating shell solvent to facilitate the process.

Fig. 2.

3.2. Fiber morphology

Both the fibers from the modified coaxial process, (F2; Fig. 3a1 and a2) and those from the modified tri-axial process (F3; Fig. 3b1 and b2) have consistent linear morphologies, with smooth surfaces and a narrow range of diameter distributions. In contrast, because of the volatile properties of acetone and ethanol, CA nanofibers from single-fluid electrospinning often have a flat morphology with wrinkled surfaces [30, 31]. These effects arise because often the surfaces of the fluid jets solidify faster than the inner parts. Subsequent evaporation of the residual solvent causes the fibers to collapse in on themselves, and results in wrinkles. In contrast, the presence of a solvent surrounding the inner fluid(s) in both the modified coaxial and tri-axial processes can promote the transfer of solvent and simultaneous solidification of the fluid jets. Thus, both fibers F2 and F3 have cylindrical morphology with smooth surfaces. They have average diameters of 0.54 ± 0.05 μm and 0.62 ± 0.07 μm, respectively, with the tri-axial fibers slightly larger than those from the coaxial process.

Fig. 3.

SEM images of the cross-sections of F2 and F3 are exhibited in Fig. 4. It is clear that the F2 fibers have a smooth cross-section without any visible particles or drug crystals embedded. In sharp contrast, there are a large number of particles present in the center of F3, suggesting the likely presence of a drug reservoir within the CA

shells.

Fig. 4.

3.3. Physical form and component compatibility

It is commonly the case that electrospun fibers with a drug homogeneously distributed in the polymer matrix are amorphous solid dispersions, which are beneficial for the dissolution of poorly water-soluble drugs [19,51]. XRD patterns of the raw materials (CA and FA) and their electrospun products are shown in Fig. 5a. The raw CA material is amorphous, as reflected by the broad humps in its XRD pattern and also the appearance of its particles under the microscope (Fig. 5b). In contrast, the raw FA particles are crystalline, with many sharp reflections in the XRD pattern. This is verified by the FA particles showing polychromic properties under polarized light (Fig. 5c).

The F2 fibers from the modified coaxial process have an XRD pattern with no characteristic reflections of crystalline FA, indicating production of an amorphous material. However, it is clear that there are still some FA reflections in the pattern of F3 (Fig. 5a). This can be ascribed to the use of a pure drug solution as the core: without the steric hindrance provided by the presence of a polymer, the FA molecules are able to re-crystallize during the process of solvent evaporation.

Fig. 5.

To explore the possibility of any secondary interactions existing between the components in the composite fibers, FTIR spectra were obtained, and are given in Fig. 6a. The molecular formulae of CA and FA are exhibited in Fig. 6b. Both CA and FA

have hydroxyl and carboxylate groups and thus can both donate and accept H-bonds.

The CA spectrum contains a characteristic -C=O absorbance peak at 1727 cm^{-1}, while FA has -C=O absorbance peaks at 1691, 1667 and 1619 cm^{-1}. Fig. 6b shows that FA molecules can potentially form two different dimers, and the presence of these in the pure drug is believed to be the reason for the three different carboxylate vibrations. These characteristic peaks have disappeared in the spectrum of F2 but can still be discerned in that of F3. In addition, the numerous sharp peaks in the fingerprint region of raw FA are absent in the F2 spectrum but can still be observed with F3. These observations suggest that the major secondary interactions present in the fibers are likely to be different. In F2, all the FA molecules were homogeneously distributed throughout the CA matrix. These FA molecules formed hydrogen bonds with the -OH or -C=O groups of CA, which hinders the formation of FA dimers and crystal lattices. In comparison, in the case of F3 most of the FA molecules were centralized in the core, and given the lack of polymer here the formation of FA dimers and a crystal lattice could occur.

Fig. 6.

3.4. In vitro drug release

FA is a typical poorly water-soluble active pharmaceutical ingredient, with a saturation solubility of 0.00583% (w/w) in water at 37 ºC [51]. Its dissolution rate is closely related to its particle size. In this work, the complete dissolution of 40 mg of FA with a particle size smaller than 20 μm took around 12 h in PBS (Fig. 7a), with 75.8 ± 5.4% of the drug freed into the bulk dissolution media in the first 4 h (Fig. 7b).

As a result of the insolubility of CA, the F2 fibers provided a sustained release profile over a time period of around 96 h (Fig. 7a). However, a significant initial burst release (27.4 ± 5.7%) within the first hour is clear (Fig. 7b), as a result of a significant proportion of the drug molecules in the fibers being close to the surface and thus able to diffuse into the release medium. This burst is even more pronounced than the raw FA (23.7 ± 6.17%). After 48 h, 88.4 ± 6.8% of the incorporated FA in F2 was released. This left a long tailing-off period, with a further 48 h required to release only 7.1% of the remaining FA.

The F3 fibers release profile is also given in Fig. 7a. F3 released only 3.7 ± 2.4% of the encapsulated FA in the first hour of the experiment, and 11.9 ± 5.1% after 2 h (Fig. 7b). After 36 h, 93.7 ± 6.4% of the FA incorporated was freed into the dissolution medium (Fig. 7a). Although both F2 and F3 were able to provide a more sustained release profile than raw FA powder (found in commercial tablets), the F3 fibers showed even better functional performance than F2. The F3 depots had no initial burst release effect, which often results in a higher blood drug concentration than the maximum safe concentration (MSC) [55]. Meanwhile, the F3 depots had less leveling-off release during the final stages of release, which often leads to a lower blood drug concentration than the minimum effective concentration (MEC) [56]. Fitting release models to the in vitro release data of F3 from 0 to 36 hours shows that FA was released in an almost zero-order manner. A linear equation between the drug release percentage (Q) and the release time (T) was calculated: Q=2.54T+8.57, with a correlation coefficient (R) of 0.9868 (Fig. 7c).

Fig. 7.

3.5. Drug release mechanism

To further explore the drug release mechanisms of F2 and F3, samples were removed from the dissolution cells and lyophilized at the end of the experiments. SEM images of the cross-sections of these samples, together with schematics of the drug distribution in the fibers, are exhibited in Fig. 8. F2 has a uniform cross-section (Fig. 8a), while F3 displays a loose, collapsed, structure in the center of the CA shell (Fig. 8b), as a result of the exhaustion of the core FA crystals.

CA is insoluble in water, and in the pharmaceutical industry is often exploited for sustained release membrane coatings or osmotic pumps [57]. Drug release from CA-based drug delivery systems (DDSs) is reported to be controlled by a typical Fickian diffusion mechanism. The Peppas equation $Q = kt^n$ can be utilized to gain more insight here. Q is the drug release percentage, t is the time, k is a constant reflecting the structural and geometric characteristics of the DDS, and n is an exponent indicating the drug release mechanism [58].

Fits of the Peppas equation to the profiles from F2 and F3 give equations of $Q_2=30.46t_2^{0.27}$ ($R_2=0.9922$) and $Q_3=5.44t_3^{0.81}$ ($R_3=0.9827$), respectively. For F2, an exponent value of 0.27 (<0.45) suggests that FA release was controlled by Fickian diffusion. For F3, an exponent value of 0.81 (<0.90, >0.45) might be interpreted to indicate that a combination of diffusion and erosion mechanisms was operational. However, it is more likely that the Peppas model is not really applicable here, since there is not a uniform distribution of the drug throughout the matrix (see Fig. 8c).

During the drug dissolution process, the insoluble CA will not degrade or abrade, and thus erosion should not occur. The composite F2 fibers do have the drug homogeneously distributed throughout the CA matrix however (Fig. 8c), and thus the Peppas equation could successfully model the release from these fibers.

Fig. 8.

Although the drug FA molecules have re-crystallized in the core of F3 (Fig. 8c), the drug release process is approximately zero-order, with no initial burst release and a very small tailing-off effect. This is thought to be because transport of FA from the central depots to the outer dissolution medium must involve three successive steps. First, water molecules must permeate to the cores of the fibers. Second, FA molecules must dissolve from the solid state into solution, and finally the free FA molecules must migrate through the CA shell to the dissolution medium. It is hypothesized that a saturated FA solution could form in the core, and since the diffusion distance to the release medium is constant (i.e. the thickness of the CA shell, T_{shell}), close to zero-order release ensues. In contrast, in the composite F2 system, the drug at the exterior of the fiber monoliths would exit first, and thus as time passes the diffusion distances will gradually increase. This leads to an accelerated burst of release at the start of the experiment, and also to the tailing off in its final stages.

We believe that the new results reported here could leads to a series of novel biomaterials aiming to provide controlled release profiles. For instance: 1) in the shell, soluble porogenic additives (such poly(ethylene glycol) or poly(vinylpyrrolidone)) could be used to regulate the drug release behavior, as is currently the case in some

particle-based drug depots [59]; 2) the approach could be extended to achieve the sustained release of soluble drugs (a major challenge in pharmaceutics); 3) drug delivery systems with more complicated drug release profiles could be achieved, e.g. multiple-phase release of a drug using a pure drug exterior compartment; 4) combined therapies with temporally sequential drug release characteristics could be explored; 5) an extremely wide range of un-spinnable fluids including dilute polymer solutions [60], surfactant or electrolyte solutions could be explored as the outer fluid in modified tri-axial processes, in order to create numerous nanoscale biomaterials with complicated nanostructures.

4. Conclusions

In this work, a modified tri-axial electrospinning process was successfully developed to generate nanoscale drug depots of ferulic acid (FA) in a cellulose acetate (CA) nanofiber. SEM images demonstrated the presence of an internal drug reservoir encapsulated by a CA shell. XRD and IR spectroscopy results verified that FA was present in the reservoirs at least in part in the crystalline form. For comparison purposes, monolithic CA/FA fibers were prepared by modified coaxial spinning, and these were found to have an amorphous distribution of drug. In vitro dissolution tests demonstrated that the core-shell depots were able to provide almost zero-order sustained release over 36 h, with no initial burst release and minimal tailing-off. The concepts demonstrated in this work pave a new way for designing advanced structural biomaterials and drug delivery systems.

Acknowledgements

This study was supported by the Natural Science Foundation of China (No.51373101), the NSFC/UK Royal Society International Exchanges Scheme (No. 51411130128/IE131748), and the Hujiang Foundation of China (No. B14006).

References

[1] Q. Hu, W. Sun, Y. Lu, H.N. Bomba, Y. Ye, T. Jiang, A.J. Isaacson, Z. Gu, Tumor microenvironment-medicated construction and deconstruction of extracellular drug-delivery depots, Nano Lett. 16 (2016) 1118-1126.

[2] F. Ramazani, C.F. Van Nostrum, G. Storm, F. Kiessling, T. Lammers, W.E. Hennink, R.J. Kok, Locoregional cancer therapy using polymer-based drug depots, Drug Discov. Today 21 (2016) 640-647.

[3] A. Flemming, Drug delivery non-invasive drug depot refill, Nat. Rev. Drug Discov. 13 (2014) 810-811.

[4] Y. Brudno, E.A. Silva, C.J. Kearney, S.A. Lewina, A. Miller, K.D. Martinick, M. Aizenberg, D.J. Mooney, Refilling drug delivery depots through the blood, Proc. Natl. Acad. Sci. USA 111 (2014) 12722–12727.

[5] A.K. Gaharwar, S.M. Mihailia, A.A. Kulkarni, A. Patel, A.D. Luca, R.L. Reis, M.E. Gomes, C.V. Blitterswijk, L. Moroni, A. Khademhosseini, Amphiphilic beads as depots for sustained drug release integrated into fibrillar scaffolds, J. Control. Release 187 (2014) 66-73.

[6] H. Liu, S.S. Venkatraman, Solid/hollow depots for drug delivery, Part 1: Effect of drug characteristics and polymer molecular weight on the phase-inversion dynamics, depot morphology and drug release, J. Pharm. Sci. 103 (2014) 485-495.

[7] D.Y. Kim, D.Y. Kwon, J.S. Kwon, J.H. Park, S.H. Park, H.J. Oh, J.H. Kim, B.H. Min, K. Park, M.S. Kim, Synergistic anti-tumor activity through combinational intratumoral injection of an in-situ injectable drug depot, Biomaterials 85 (2016) 232-245.

[8] J. Di, S. Yao, Y. Ye, Z. Cui, J. Yu, T.K. Ghosh, Y. Zhu, Z. Gu, Stretch-triggered drug delivery from wearable elastomer films containing therapeutic depots. ACS Nano 9 (2015) 9407-9415.

[9] C.J. Carling, M.L. Viger, V.A.N. Huu, A.V. Garcia, A. Almutairi, In vivo visible light-triggered drug release from an implanted depot. Chem. Sci. 6 (2015) 335-341.

[10] H.W. Seo, D.Y. Kim, D.Y. Kwon, L.M. Jin, B. Lee, J.H. Kim, B.H. Min, M.S. Kim, Injectable intratumoral hydrogel as 5-fluorouracil drug depot, Biomaterials 34 (2013) 2748-2757.

[11] C.J. Kastrup, M. Nahrendor, J.L. Figueiredo, H. Lee, S. Kambhampati, T. Lee, S.W. Cho, R. Gorbatov, Y. Iwamoto, T.T. Dang, et al, Painting blood vessels and atherosclerotic plaques with an adhesive drug depot, Proc. Natl. Acad. Sci. USA 109 (2012) 21444-21449.

[12] M. Singhal, S. Del Rio-Sancho, K. Sonaje, Y.N. Kalia, Fractional laser ablation for the cutaneous delivery of triamcinolone acetonide from cryomilled polymeric microparticles: creating intraepidermal drug depots, Mol. Pharm. 13 (2016) 500-511.

[13] Y. Brudno, D.J. Mooney, On-demand drug delivery from local depots, J. Control. Release 219 (2015) 8-17.

[14] X. Lin, Y. Xu, X. Tang, Y. Zhang, J. Chen, Y. Zhang, H. He, Z. Yang, A uniform ultra-small microsphere/SAIB hybrid depot with low burst release for long-term continuous drug release, Pharm. Res. 32 (2015) 3708-3721.

[15] S. Supper, N. Anton, J. Boisclair, N. Seidel, M. Riemenschnitter, C. Curdy, T. Vandamme, Chitosan/glucose 1-phosphate as new stable in situ forming depot system for controlled drug delivery. Eur. J. Pharm. Biopharm. 88 (2014) 361-373.

[16] C.C. Huang, W.T. Chia, M.F.bChung, K.J. Lin, C.W. Hsiao, C. Jin, W.H. Lim, C.C. Chen, H.W.Sung, An implantable depot that can generate oxygen in situ for overcoming hypoxia-induced resistance to anticancer drugs in chemotherapy, J. Am. Chem. Soc. 138 (2016) 5222-5225.

[17] C. Manaspon, S. Hongeng, A. Boongird, N. Nasongkla, Preparation and in vitro characterization of SN-38-loaded, self-forming polymeric depots as an injectable drug delivery system, J. Pharm. Sci. 101 (2012) 3708-3717.

[18] C. Delplace, F. Kreye, D. Klose, F. Danède, M. Descamps, J. Siepmann, F. Siepmann, Impact of the experimental conditions on drug release from parenteral depot systems: From negligible to significant. Int. J. Pharm. 432 (2012) 11-22.

[19] Z.K. Nagy, A. Balogh, B. Démuth, H. Pataki, T. Vigh, B. Szabó, K. Molnár, B.T. Schmidt, P. Horák, G. Marosi, G. Verreck, I.V. Assche, M.E. Brewste, High speed electrospinning for scaled-up production of amorphous solid dispersion of itraconazole, Int. J. Pharm. 480 (2015) 137-142.

[20] D.W. Song, S.H. Kim, H.H. Kim, K.H. Lee, C.S. Ki, Y.H. Park, Multi-biofunction of antimicrobial peptide-immobilized silk fibroin nanofiber membrane: Implications for wound healing, Acta Biomater. 39 (2016) 146–155

[21] K. Shimomura, A.C. Bean, H. Lin, N. Nakamura, R.S. Tuan, In vitro repair of meniscal radial tear using aligned electrospun nanofibrous scaffold, Tissue Eng. A 21 (2015) 2066-2075.

[22] S.C. Sundararaj, M.Al-Sabbagh, C.L. Rabek, T.D. Dziubla, M.V. Thomas, D.A. Puleo,Comparison of sequential drug release in vitro and in vivo. J. Biomed. Mater. Res. B Appl. Biomateri. 104 (2016) 1302-1310.

[23] S. Jiang, G. Duan, E. Zussman, A. Greiner, S. Agarwal, Highly flexible and tough concentric tri-axial polystyrene fibers. ACS Appl. Mater. Interfaces 6 (2014) 5918-5923.

[24] S. Labbaf, H. Ghanbar, E. Stride, M. Edirisinghe, Preparation of multilayered polymeric structures using a novel four-needle coaxial electrohydrodynamic device, Macromol. Rapid Commun. 35 (2014) 618-623.

[25] G. Chen, Y. Xu, D.G. Yu, D.F. Zhang, N.P. Chatterton, K.N. White, Structure-tunable Janus fibers fabricated using spinnerets with varying port

angles, Chem. Commun. 51 (2015) 4623-3626.

[26] G. Yang, H. Lin, B.B. Rothrauff, S. Yu, R.S. Tuan, Multilayered polycaprolactone/gelatin fiber-hydrogel composite for tendon tissue engineering, Acta Biomater. 35 (2016) 68-76.

[27] C.L. He, Z.M. Huang, X.J. Han, Fabrication of drug-loaded electrospun aligned fibrous threads for suture applications. J Biomedical Mater Res A 89(2009)80-95.

[28] C. Yang, D.G. Yu, D. Pan, X.K. Liu, X. Wang, S.W.A. Bligh, G.R. Williams, Electrospun pH-sensitive core-shell polymer nanocomposites fabricated using a tri-axial processes, Acta Biomater. 35 (2016) 77-86.

[29] H.F. Wen, C. Yang, D.G. Yu, X.Y. Li, D.F. Zhang, Electrospun zein nanoribbons for treatment of lead-contained wastewater, Chem. Eng. J. 290 (2016) 263-272.

[30] D.G. Yu, J.H. Yu, L. Chen, G.R. Williams, X. Wang, Modified coaxial electrospinning for the preparation of high-quality ketoprofen-loaded cellulose acetate nanofibers, Carbohydr. Polym. 90 (2012) 1016-1023.

[31] D.G. Yu, J.H. Yu, L. Chen, G.R. Williams, X. Wang, Modified coaxial electrospinning for the preparation of high-quality ketoprofen-loaded cellulose acetate nanofibers, Carbohydr. Polym. 90 (2012) 1016-1023.

[32] D.G. Yu, X.Y. Li, X. Wang, J.H. Yang, S.W.A. Bligh, G.R. Williams, Nanofibers fabricated using tri-axial electrospinning as zero order drug delivery systems, ACS Appl. Mater. Interfaces 7 (2015) 18891-18897.

[33] V. Kalra, J.H. Lee, J.H. Park, M. Marquez, Y.L. Joo, Confined assembly of asymmetric block‐copolymer nanofibers via multiaxial jet electrospinning, Small 5 (2009) 2323-2332.

[34] E. Hosono, Y.G. Wang, N. Kida, M. Enomoto, N. Kojima, M. Okubo, H. Matsuda, Y. Saito, T. Kudo, I. Honma, Synthesis of triaxial LiFePO4 nanowire with a VGCF core column and a carbon shell through the electrospinning method, ACS Appl. Mater. Interfaces 2 (2010) 212-218.

[35] D. Han, A.J. Steckl, Triaxial electrospun nanofiber membranes for controlled dual release of functional molecules, ACS Appl. Mater. Iinterfaces 5 (2013) 8241-8245.

[36] W. Liu, C. Ni, D.B. Chase, J.F. Rabolt, Preparation of multilayer biodegradable nanofibers by triaxial electrospinning, ACS Macro Lett. 2 (2013) 466-468.

[37] J.S.M. Zanjani, B.S. Okan, I. Letofsky-Papst, M. Yildiz, Y.Z. Menceloglu, Rational design and direct fabrication of multi-walled hollow electrospun fibers with controllable structure and surface properties, Eur. Polym. J. 62 (2015) 66-76.

[38] J.S.M. Zanjani, B.S. Okan, I. Letofsky-Papst, Y.Menceloglu, M. Yildiz, Repeated self-healing of nano and micro scale cracks in epoxy based composites by tri-axial electrospun fibers including different healing agents, RSC Adv. 5 (2015) 73133-73145.

[39] J.S.M. Zanjani, B.S. Okan, Y.Z. Menceloglu, M. Yildiz, Design and fabrication of multi-walled hollow nanofibers by triaxial electrospinning as reinforcing agents in nanocomposites, J. Reinf. Plast. Comp. 34 (2015) 1273-1286.

[40] A. Khalf, K. Singarapu, S.V. Madihally, Influence of solvent characteristics in triaxial electrospun fiber formation, React. Funct. Polym. 90 (2015) 36-46.

[41] W.K. Fong, T.L. Hanley, B. Thierry, A. Hawley, B.J. Boyd, C.B. Landersdorfer, External manipulation of nanostructure in photoresponsive lipid depot matrix to control and predict drug release in vivo, J. Control. Release 228 (2016) 67-73.

[42] R.W. Kalicharan, P. Schot, H. Vormans, Fundamental understanding of drug absorption from a parenteral oil depot, Eur. J. Pharm. Sci. 83 (2016) 19-27.

[43] A. Fakhari, J.A. Subramony, Engineered in situ depot-forming hydrogels for intratumoral drug delivery, J. Control. Release 220 (2015) 465-475.

[44] K.S. Brammer, S. Oh, J.O. Gallagher, S. Jin, Enhanced cellular mobility guided by TiO_2 nanotube surfaces, Nano Lett. 8 (2008) 786-793.

[45] S.C. Sundararaj, M.V. Thomas, T.D. Dziubla, D.A. Puleo, Bioerodible system for sequential release of multiple drugs, Acta Biomater. 10 (2014) 115-125.

[46] A. Rezaei, A. Nasirpour, M. Fathi, Application of cellulosic nanofibers in food science using electrospinning and its potential risk, Compr. Rev. Food Sci. F. 14 (2015) 269-284.

[47] I. Siró, D. Plackett, Microfibrillated cellulose and new nanocomposite materials: a review. Cellulose 17 (2010) 459-494.

[48] R. Konwarh, N. Karak, M. Misra, Electrospun cellulose acetate nanofibers: the present status and gamut of biotechnological applications, Biotechnol. Adv. 31 (2013) 421-437.

[49] X.M. Wu, C. Branford-White, L.M. Zhu, N.P. Chatterton, D.G. Yu, Ester prodrug-loaded electrospun cellulose acetate fiber mats as transdermal drug delivery systems, J. Mater. Sci. Mater. Med. 21 (2010) 2403-2411.

[50] K. Ohkawa, Nanofibers of cellulose and its derivatives fabricated using direct electrospinning, Molecules, 20 (2015) 9139-9154.

[51] D.G. Yu, J.M. Yang, C. Branford-White, P. Lu, L. Zhang, L.M. Zhu, Third generation solid dispersions of ferulic acid in electrospun composite nanofibers, Int. J. Pharm. 400 (2010) 158-164.

[52] R.G. Chaudhuri, S. Paria, Core/shell nanoparticles: classes, properties, synthesis mechanisms, characterization, and applications, Chem. Rev. 112 (2012) 2373-2433.

[53] A. Greiner, J.H. Wendorff, Electrospinning: a fascinating method for the preparation of ultrathin fibers, Angew Chem. Int. Ed. 46 (2007) 5670-5703.

[54] C. Li, Z.H. Wang, D.G. Yu, G.R. Williams, Tunable biphasic drug release from ethyl cellulose nanofibers fabricated using a modified coaxial electrospinning process, Nanoscale Res. Lett. 9 (2014) 258.

[55] Y. Malam, M. Loizidou, A.M. Seifalian, Liposomes and nanoparticles: nanosized vehicles for drug delivery in cancer, Trends pharmacol. Sci. 30 (2009) 592-599.

[56] G. Acharya, K. Park, Mechanisms of controlled drug release from drug-eluting stents, Adv. Drug del. Rev. 58 (2006) 387-401.

[57] C. Bindschaedler, R. Gurny, E. Doelker, Osmotically controlled drug delivery systems produced from organic solutions and aqueous dispersions of cellulose acetate. J. Control. Release 4 (1986) 203-212.

[58] N.A. Peppas, Analysis of Fickian and non-Fickian drug release from polymers, Pharm, Acta Hel. 60 (1985) 110-111.

[59] H.M. Hsiao, Y.H. Chiu, T.Y. Wu, J.K. Shen, T.Y. Lee, Effects of through-hole drug reservoirs on key clinical attributes for drug-eluting depot stent, Med. Eng. Phys. 35 (2013) 884-897.

[60] F. Xu,Y. Xu, D. Yu, Zero-order controlled release nanofibers fabricated using coaxial electrospinning with polymer dilute solution as a sheath fluid. J. Uni. Shanghai Sci. Technol. 37 (2015) 165-168.

Table and Figure Legends

Table 1. Experimental parameters used for creating different types of drug-loaded nanofibers.

Fig. 1. Schematics showing the electrospinning process. (a) The key features of the experiment, illustrating the different spinnerets used for single-fluid, coaxial and tri-axial spinning. (b) A schematic diagram depicting the working fluids used in tri-axial spinning in this work.

Fig. 2. Digital images of the concentric spinneret (a1 and a2) and tri-layer concentric spinneret (a3 and a4), and typical observations during the (b) traditional coaxial, (c) modified coaxial and (d, e) tri-axial processes. The bottom-right inset of (e) shows the compound tri-axial Taylor cone.

Fig. 3. SEM images of the composite nanofibers from modified coaxial spinning (F2; a1 and a2) and the core-shell fibers from the modified tri-axial process (F3; b1 and b2).

Fig. 4. SEM images of the cross-sections of F2 (a1 and a2) and F3 (b1 and b2).

Fig. 5. (a) XRD patterns of the raw materials, F2 and F3; and, images taken under polarized light of (b) CA and (c) FA.

Fig. 6. (a) FTIR spectra of CA, FA, F2 and F3 and (b) molecular formulae and an illustration of the hydrogen bonding possible between FA molecules.

Fig. 7. The in vitro dissolution profiles of FA particles, F2 and F3 over (a) 96h and (b) the early stages of the release experiment, with (c) the results of fitting a zero-order profile to the data for F3.

Fig. 8. Typical SEM images of the cross-sections of the remains of (a) F2 and (b) F3 after drug exhaustion. (c) A schematic diagram of the drug distributions in the CA matrices, and their different mechanisms controlling their release behavior.

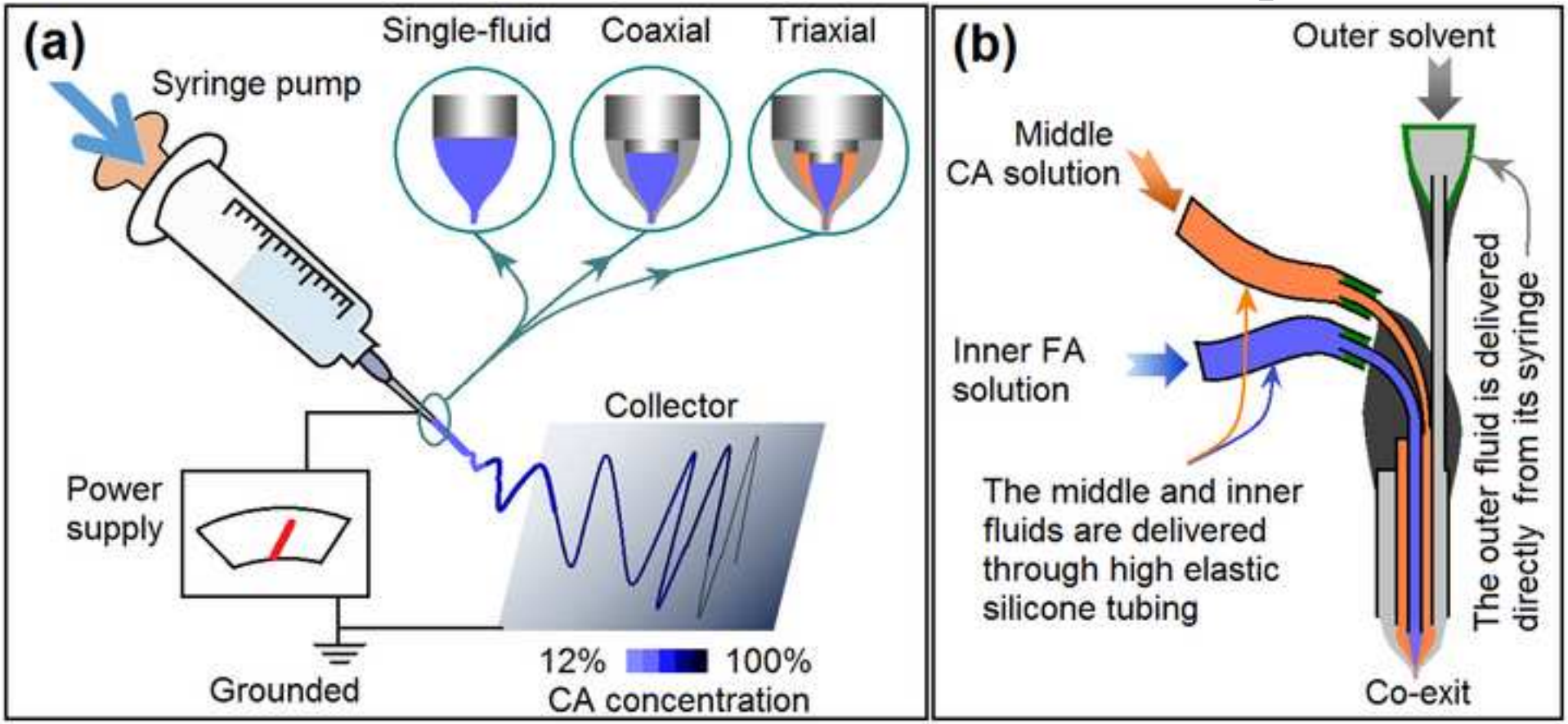
(a)
Single-fluid
Coaxial
Triaxial
Syringe pump
Collector
Power supply
Grounded
12%
100%
CA concentration
(b)
Outer solvent
Middle CA solution
Inner FA solution
The middle and inner fluids are delivered through high elastic silicone tubing
The outer fluid is delivered directly from its syringe
Co-exit

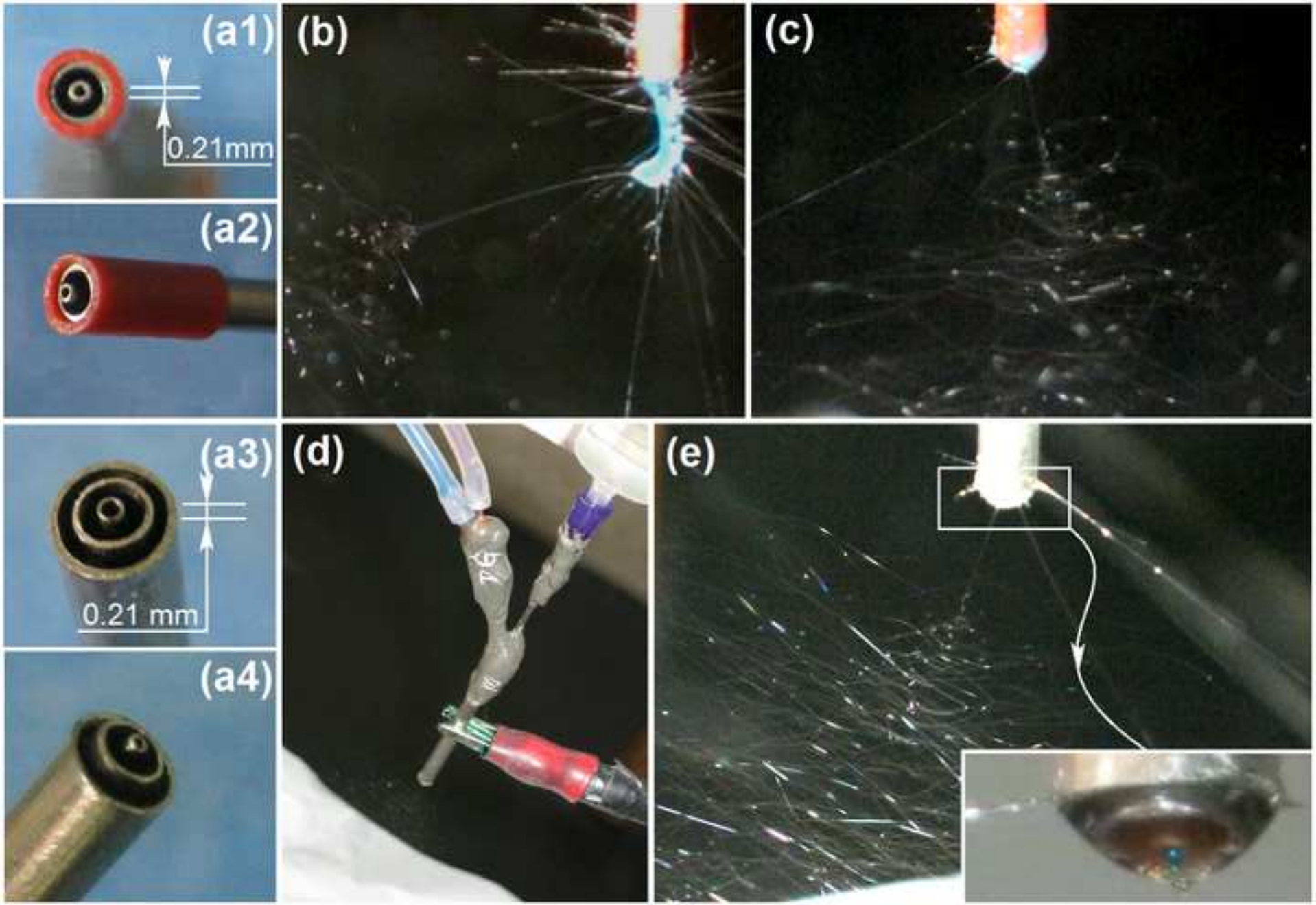

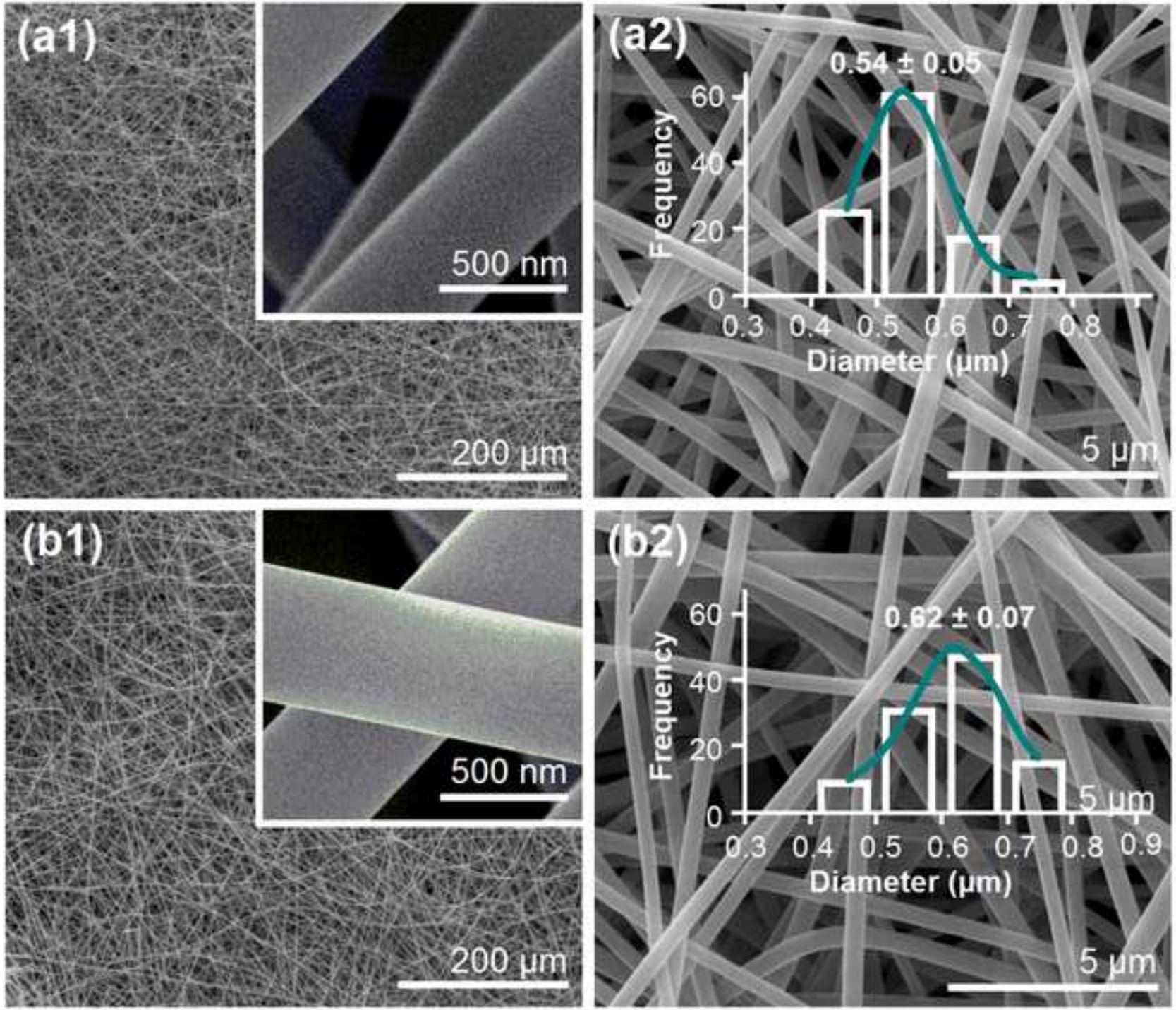

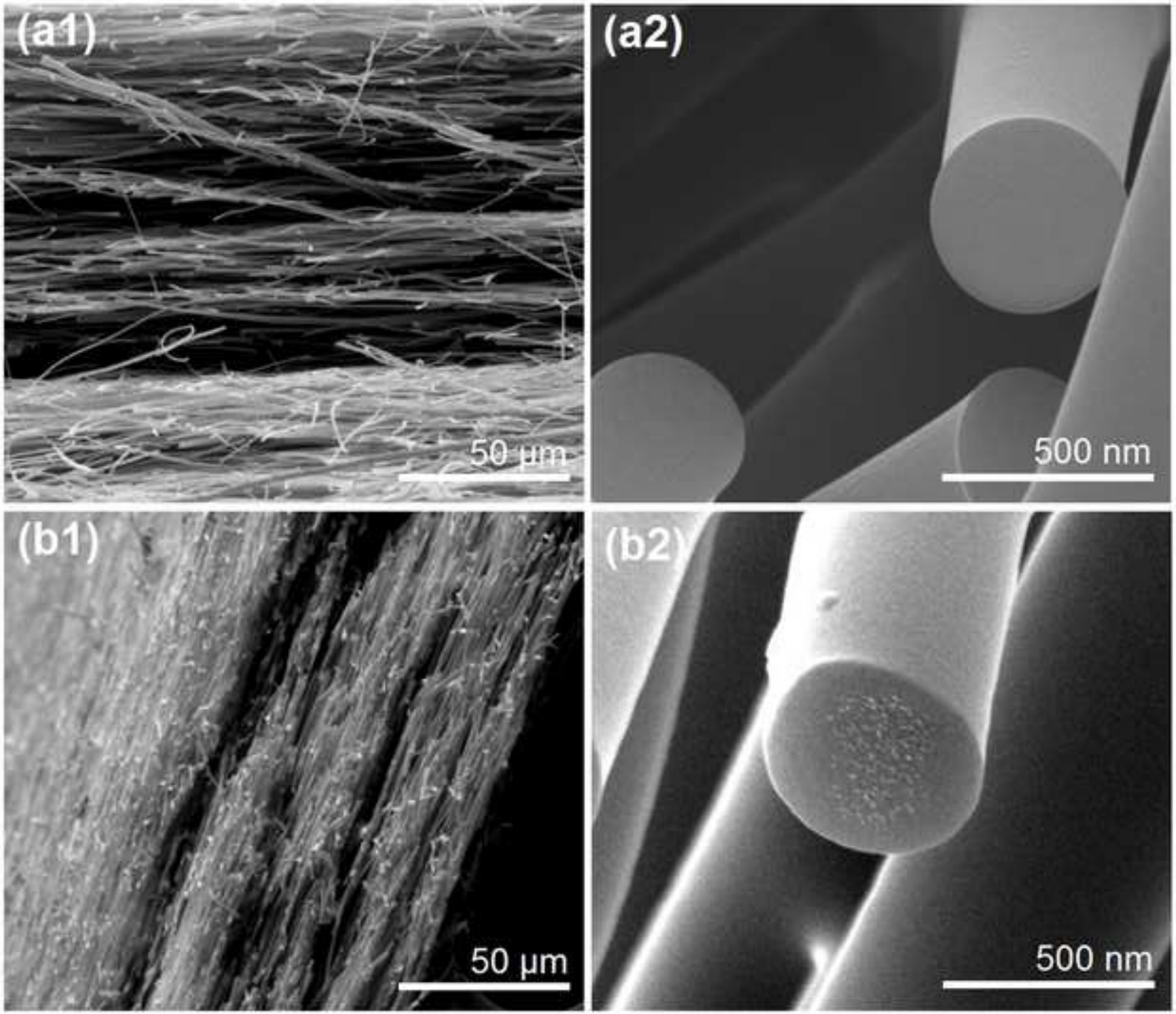

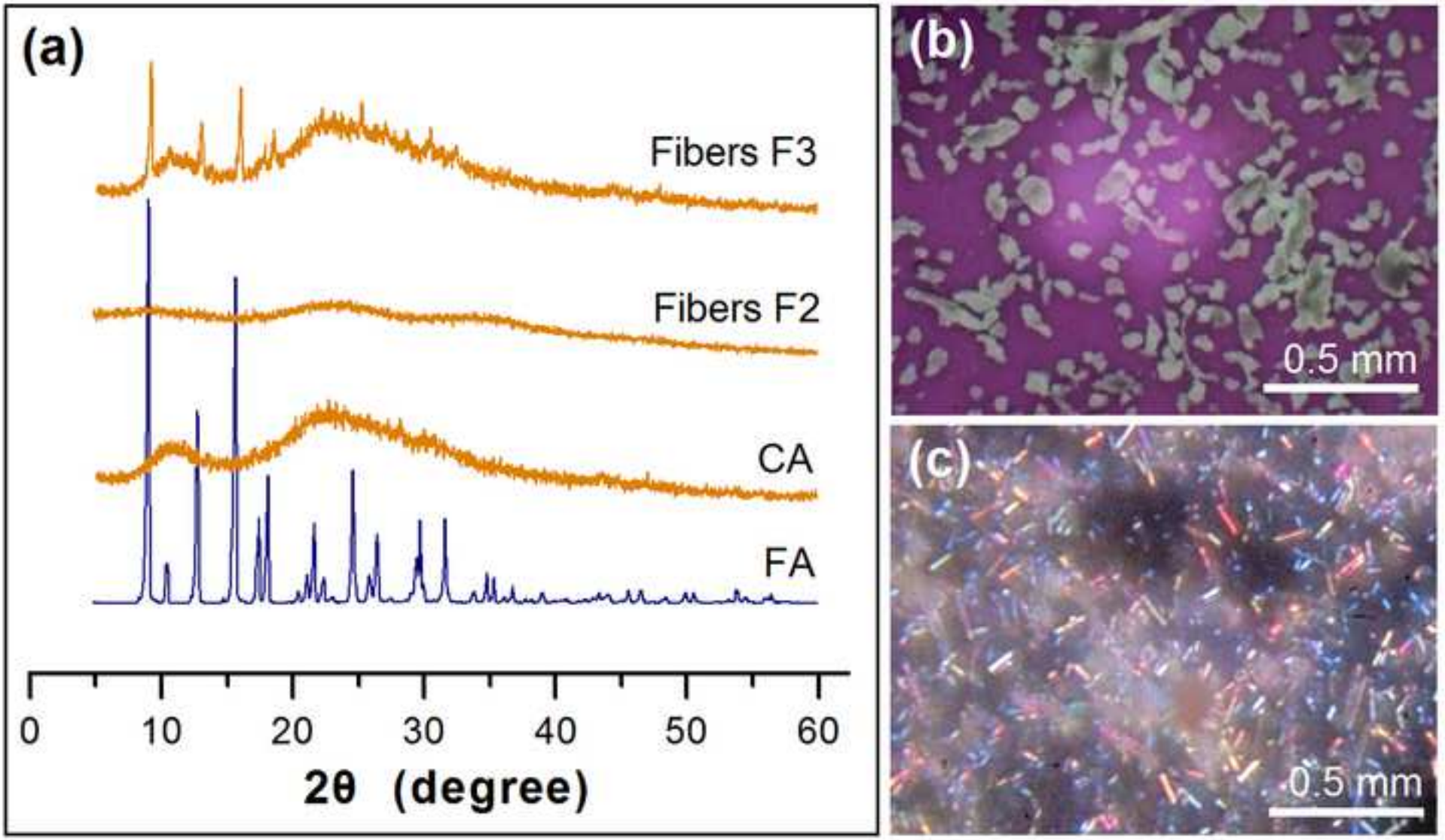
(a)
Fibers F3
Fibers F2
CA
FA
0
10
20
30
40
50
60
2θ (degree)
(b)
0.5 mm
(c)
0.5 mm

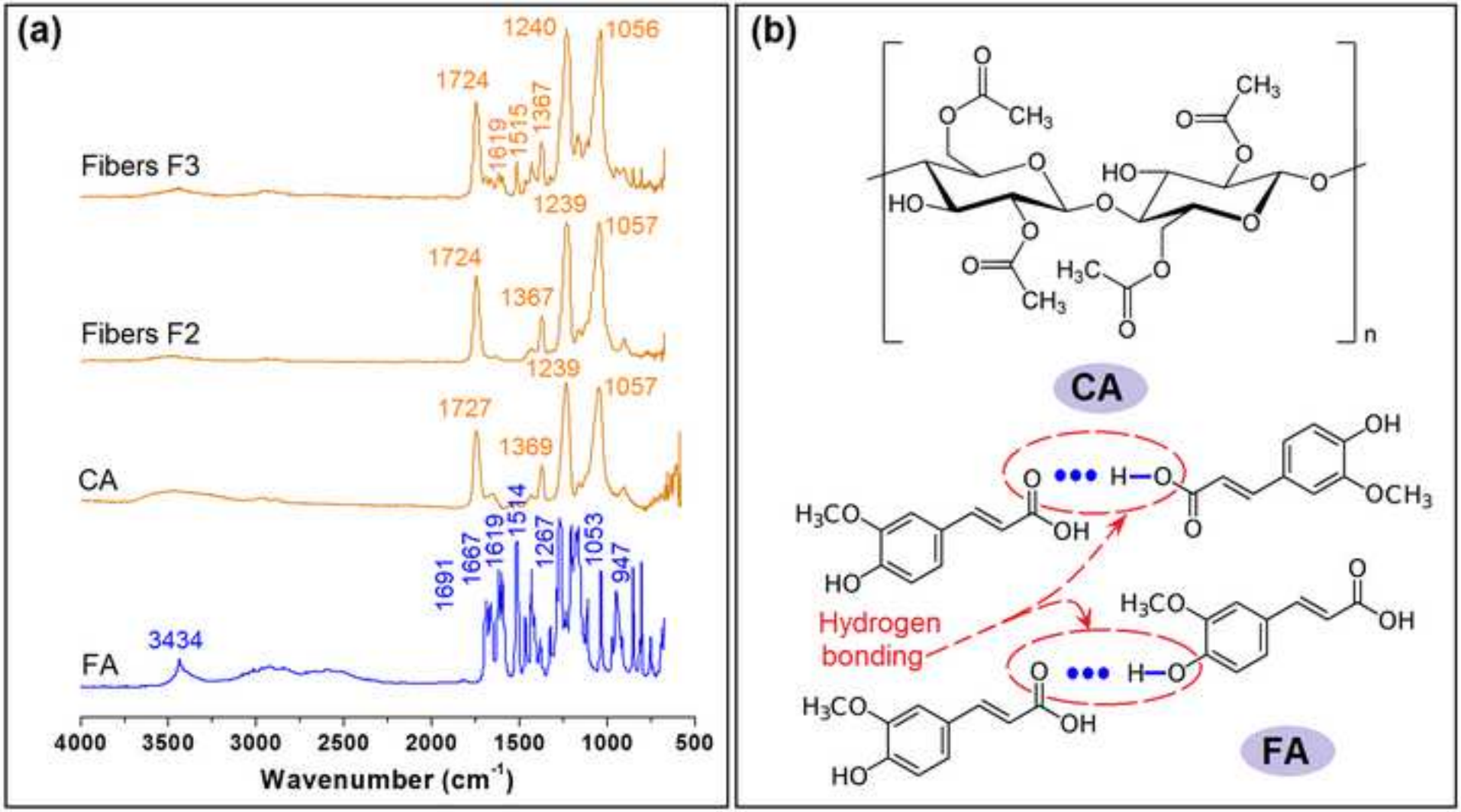

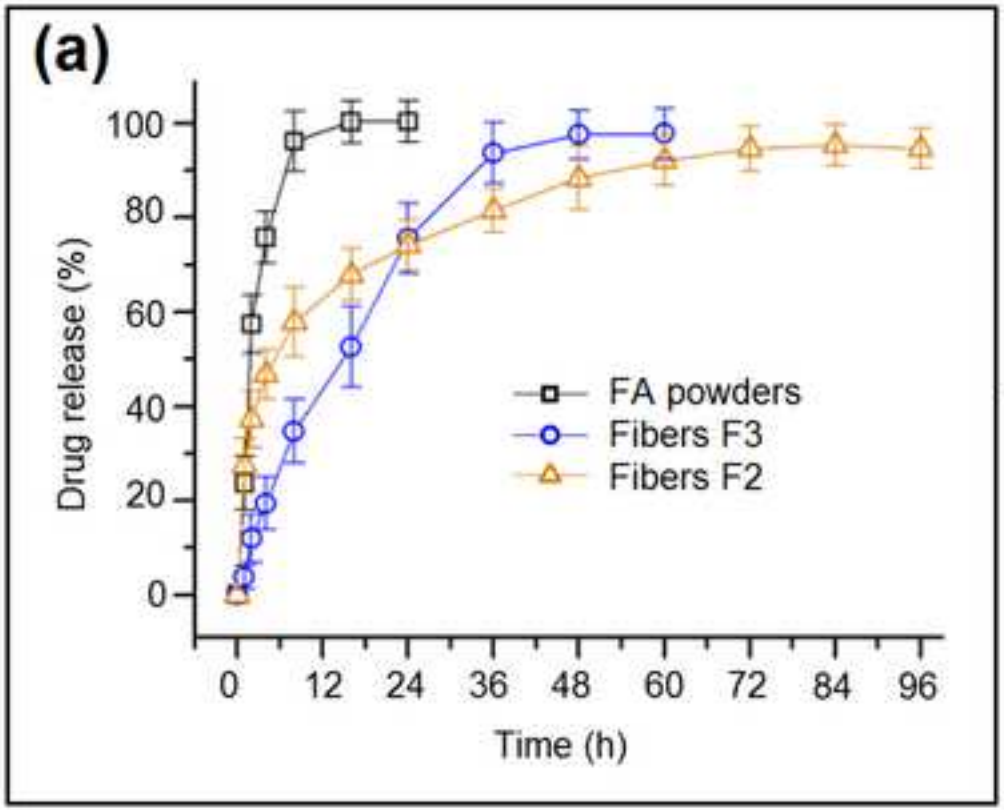

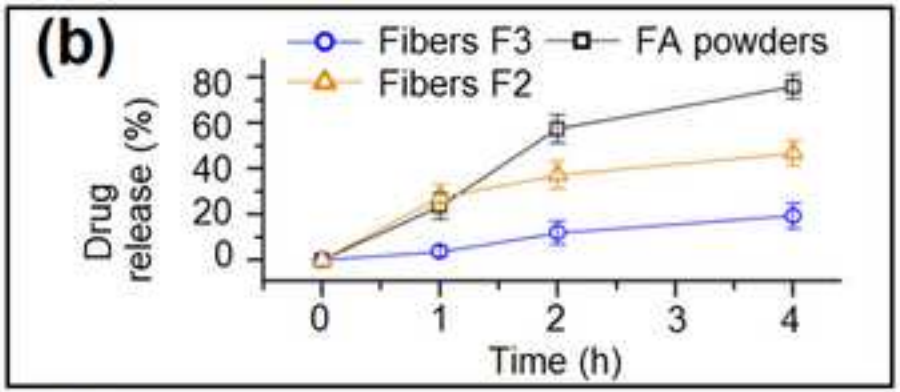

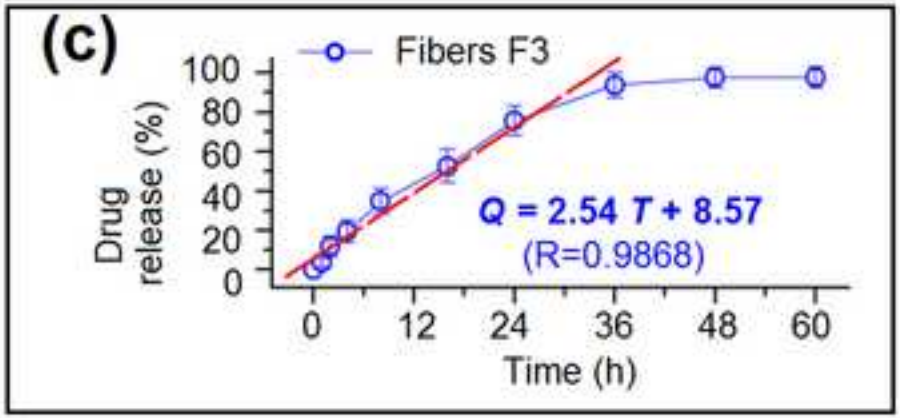

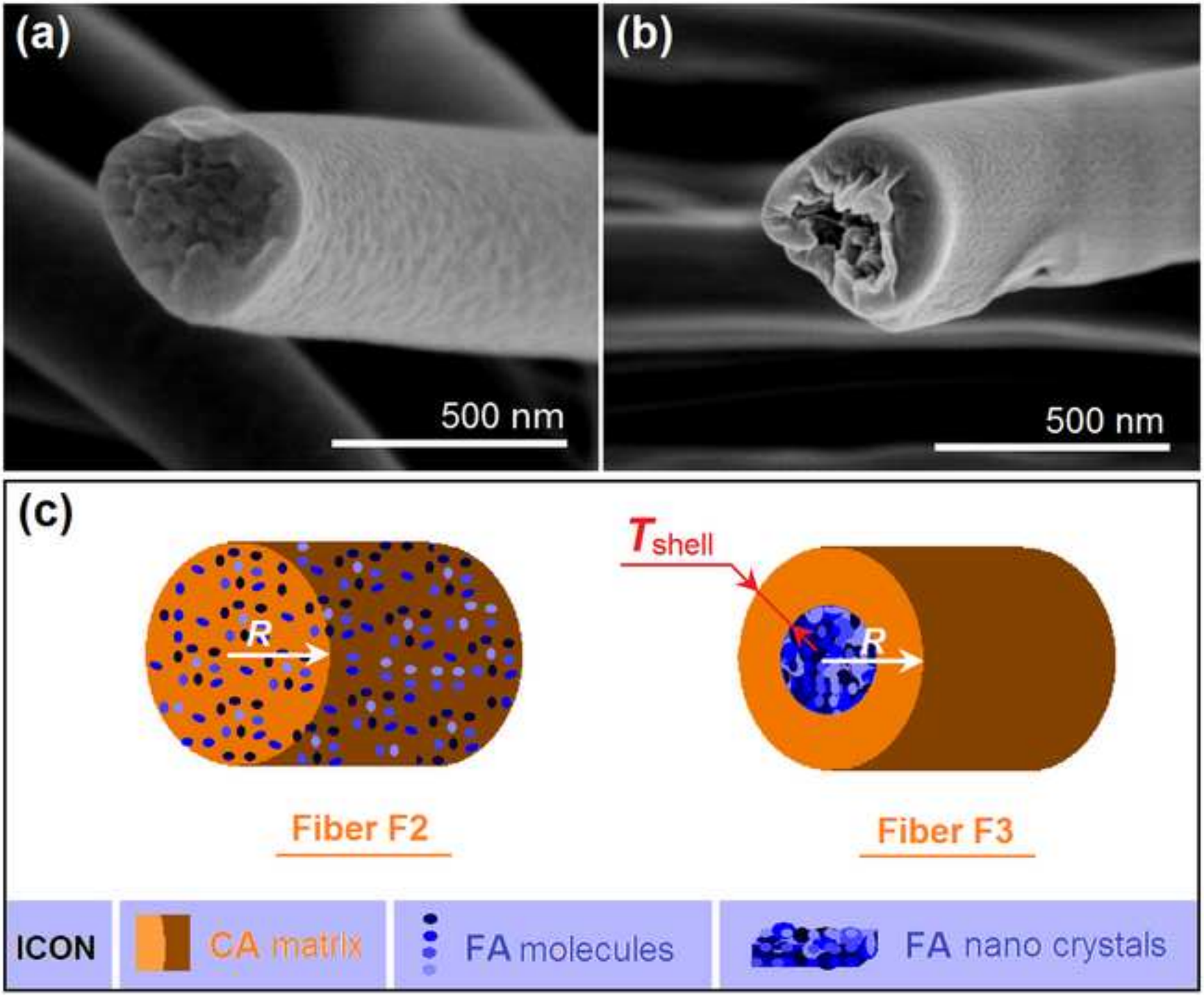

Table1 Experimental parameters used for creating different types of drug-loaded nanofibers

No.	Process	Working fluid			Outer/Middle/Inner fluid flow rate (mL/h)	Theoretical drug loading (% w/w)
		Outer	Middle	Inner		
F1	Coaxial	CA solution [a]	--	FA solution [b]	2.0/--/0.4	20
F2	Modified coaxial	Mixed solvent-only [c]	--	CA and FA mixed solution [d]	0.5/--/2.4	20
F3	Modified tri-axial		CA solution [a]	FA solution [b]	0.5/2.0/0.4	20

[a] The CA solution consisted of 12% (w/v) CA in a mixture of acetone:ethanol:DMAc (4:1:1, v:v:v);
[b] The FA solution consisted of 15% (w/v) FA in a mixture of acetone:ethanol:DMAc (4:1:1, v:v:v);
[c] The mixed solvent was a mixture of acetone:ethanol:DMAc (4:1:1, v:v:v);
[d] The CA and FA mixed solution consisted of 12% (w/v) CA and 3.0% (w/v) FA in a mixture of acetone:ethanol:DMAc (4:1:1, v:v:v).

Graphical abstract

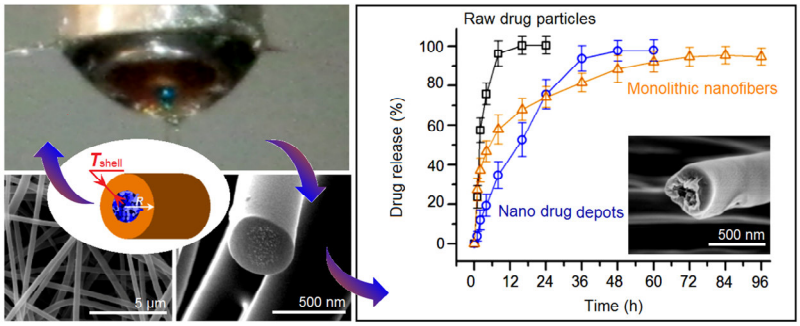

Statement of Significance (limited to 120 words)

Nano drug depot with a drug reservoir surrounded by the drug carrier is a highly attractive topic in biomedical fields presently. A cellulose acetate based drug depot was investigated in details, including the design of nanostructure, its fabrication using a modified tri-axial electrospinning process, and a series of characterizations. The core-shell fiber-based drug depots can provide better long-time drug sustained release profile with no initial burst effect and less tailing-off release than its counterpart, the electrospun monolithic medicated nanofibers. The drug controlled release mechanism is distinct. This proof-of-concept job can be further expanded to conceive a series of new kinds of structural biomaterials with improved or new functional performances.